Nano Research
2020, 13(10): 2803–2811
ISSN 1998-0124 CN 11-5974/O4
https://doi.org/10.1007/s12274-020-2932-4

Research Article

Construction of self-sensitized $LiErF_4$: 0.5% Tm^{3+}@$LiYF_4$ upconversion nanoprobe for trace water sensing

Ling Zhang[1], Xiaodan Li[2], Wang Wang[3], Xu Zhao[1], Xu Yan[1], Chenguang Wang[1], Haoqiang Bao[1], Yang Lu[1], Xianggui Kong[3], Fengmin Liu[1], Xiaomin Liu[1] (✉), and Geyu Lu[1] (✉)

[1] *State Key Laboratory of Integrated Optoelectronics, Jilin Key Laboratory of Advanced Gas Sensors, College of Electronic Science and Engineering, Jilin University, Changchun 130012, China*
[2] *Department of Respiratory Medicine, The First Hospital, Jilin University, Changchun 130021, China*
[3] *State Key Laboratory of Luminescence and Applications, Changchun Institute of Optics, Fine Mechanics and Physics, Chinese Academy of Science, Changchun 130033, China*

Received: 4 April 2020 / **Revised:** 6 June 2020 / **Accepted:** 13 June 2020

ABSTRACT

$LiErF_4$ was commonly used as a dipolar-coupled antiferromagnet, and was rarely considered as a luminescent material. Herein, we achieved the strong red upconversion emission of $LiErF_4$ simply by an inert shell coating, i.e., $LiErF_4$@$LiYF_4$. Owing to the unique and intrinsic ladder-like energy levels of Er^{3+} ions, this $LiErF_4$ core–shell nanostructures present red emission (~ 650 nm) under multi-band excitation in the near-infrared (NIR) region (~ 808, ~ 980, and ~ 1,530 nm). A brighter and monochromic red emission can be further obtained via doping 0.5% Tm^{3+} into the $LiErF_4$ core, i.e., $LiErF_4$: 0.5% Tm^{3+}@$LiYF_4$. The enriched Er^{3+} ions and strong monochromic red emission natures make $LiErF_4$: 0.5% Tm^{3+}@$LiYF_4$ nanocrystals very sensitive for trace water probing in organic solvents with detection limit of 30 ppm in acetonitrile, 50 ppm in dimethyl sulfoxide (DMSO), and 58 ppm in *N*, *N*-dimethylformamide (DMF) under excitation of 808 nm. Due to their superior chemical and physical stability, these nanoprobes exhibit excellent antijamming ability and recyclability, offering them suitable for real-time and long-term water monitoring.

KEYWORDS

$LiErF_4$, water detection, upconversion emission, sensor, self-sensitized

1 Introduction

Water is the source of life. However, it is considered as an impurity and contaminant in some cases. For example, in organic solvent, the presence of water can lead to catastrophic failures, such as fires and explosions under some circumstances. In petroleum industry, the presence of water may cause a drop in engine' s performance, resulting in engine damage [1, 2]. Hence, the detection and quantification of trace water is a crucial matter not only in the aforementioned aspects, but also in pharmaceuticals, electronics, and food processing [3].

The primary standard for water detection in sample substances is the highly sensitive Karl Fischer coulometric titration method [4]. However, it has several disadvantages including the use of toxic and expensive chemical reagents, long measuring time, and inability of real-time monitoring [5]. Recently, fluorescence-based optical water sensors appear to be particularly attractive on account of their highly sensitive and selective, easy to fabricate, as well as their capability of remote and *in situ* monitoring [6–9]. Despite the advance, the majority of the optical water sensors focus on organic luminescent molecules, which suffer from poor reusability and photo instability [10, 11]. As an alternative, the inorganic materials represented by lanthanide doped upconversion nanoparticles (Ln-UCNPs) show their excellent performance in the field of water detection [12–14].

Ln-UCNPs have been extensively studied for their potential detection applications owing to their unique optical properties, such as large anti-Stokes shift, sharp emission, high penetration depth, low toxicity, weak background autofluorescence, and high photostability [15–21]. The luminescence of Ln-UCNPs can be easily quenched by water molecules, which provide the basis for water probing [22, 23]. For example, in the typical sensitizer Yb^{3+} and activator Er^{3+} co-doped UCNPs, e.g., 18% Yb^{3+}, 2% Er^{3+}: $NaYF_4$, the OH-vibrations of the water molecules absorbed on the surface of the UCNPs result in the quenching of the luminescence of Er^{3+} ions. In addition, the absorption of Yb^{3+} ions at 980 nm overlaps that of water molecules, leading to the excitation energy depletion, making them a good candidate for water sensing [12]. However, for the detection of water within organisms or organic solvents, the overheating effect induced by the strong absorption of water molecules at 980 nm excitation is harmful. Considering the large absorption cross-section of Nd^{3+} at 808 nm and the efficient energy transfer from excited Nd^{3+} to Yb^{3+} ions, the Nd^{3+} and Yb^{3+} co-operative sensitized UCNPs, e.g., 20% Yb^{3+}, 1% Er^{3+}: $NaGdF_4$@20% Yb^{3+}, 10% Nd^{3+}: $NaYF_4$, were subsequently reported for 808 nm triggered water probing [13]. However, it should be noted that the doping concentration of Er^{3+} in all these reported nanoprobes are no more than 2% because of the concentration quenching effect [24, 25], which seriously limit the number of the detector Er^{3+} ions, thus substantially restricting their detection sensitivity.

Address correspondence to Xiaomin Liu, xiaominliu@jlu.edu.cn; Geyu Lu, lugy@jlu.edu.cn

Very recently, we, along with other researchers, have discovered an activator Er^{3+} ions fully doped upconversion nano-system, e.g., $NaErF_4$@$NaYF_4$, completely eliminating the concentration quenching effect [26–28]. Although the use of Na-based lanthanide host matrices ($NaLnF_4$) has been considered as an efficient way to obtain upconversion emission and has been widely explored for most UCNPs, Li-based $LiLnF_4$ UCNPs are on-par in light upconversion efficiency and in certain cases are more preferable than Na-based counterparts [29–32]. As far as the chemical composition was concerned, $NaErF_4$ and $LiErF_4$ are similar to each other, and it seems that $LiErF_4$ can be obtained by simply substituting Na^+ with Li^+. However, the crystal structure of $NaErF_4$ is different from that of $LiErF_4$ (the former has hexagonal structure, while the latter has tetragonal structure) [33, 34], resulting in development of different morphologies during growth (the former shows hexagonal shape and the latter exhibits tetragonal bipyramidal shape) [29, 35]. Thus, they are completely different from the viewpoint of crystal structure and morphology despite their similar chemical composition. Moreover, up to now, $LiErF_4$ material was mainly studied as a dipolar-coupled antiferromagnet [36, 37], but few reports focus on its emission property.

Herein, we developed a strong red upconversion emission $LiErF_4$ nano-system, i.e., $LiErF_4$@$LiYF_4$ and its relevant derivative $LiErF_4$: 0.5% Tm^{3+}@$LiYF_4$, where Er^{3+} ions act as both activator and sensitizer. Owing to the unique and intrinsic ladder-like energy levels of Er^{3+} ions, these $LiErF_4$ core–shell nanostructures present red emission (~ 650 nm) under multi-band excitation in the near-infrared (NIR) region (~ 808, ~ 980, and ~ 1,530 nm), unlike the traditional sensitizer and activator co-doping systems which were only triggered by one specific wavelength. Through introducing 0.5% Tm^{3+} as a transient energy trapping center into the $LiErF_4$ core to confine the excitation energy and minimize the energy loss caused by the rapid migration between Er^{3+} ions, a brighter and monochromic red emission can be further achieved. The enriched Er^{3+} ions and strong monochromic red emission natures make $LiErF_4$: 0.5% Tm^{3+}@$LiYF_4$ nanoparticles very sensitive for trace water sensing in organic solvent with the detection limit of 30 ppm in acetonitrile, 50 ppm in dimethyl sulfoxide (DMSO), and 58 ppm in *N*, *N*-dimethylformamide (DMF) under excitation of 808 nm. Due to their superior chemical and physical stability, these probes exhibit excellent antijamming ability and recyclability, affording them suitable for real-time and long-term water monitoring.

2 Experimental section

2.1 Materials

$ErCl_3·6H_2O$ (99.9%), $YCl_3·6H_2O$ (99.9%), $TmCl_3·6H_2O$ (99.9%), oleic acid (OA, 90%), 1-octadecene (ODE, 90%), and $NOBF_4$ (95%) were purchased from Sigma-Aldrich. LiOH (anhydrous, 98%) was purchased from Aladdin. NH_4F (> 96%) was purchased from Xilong Scientific. DMF (99.8%, Super Dry), DMSO (99.9%, Super Dry), and acetonitrile (99.9%, Super Dry) were purchased from J&K Scientific. All reagents were directly used without further purification.

2.2 Measurements

The crystal structure of upconversion nanoparticles was obtained by Rigaku wide-angle X-ray diffractometer (XRD, D/max rA, using Cu Kα radiation at wave length 1.5406 Å) in the angular range of 10°–80°. The detailed structure and morphology of the nanoparticles were obtained by JEM-2100 transmission electron microscope (TEM). The upconversion emission spectra were measured at room temperature by FL920 Spectrometer (EDINBURGH). The excitation source is 808, 980, and 1,535 nm semiconductor laser (all were purchased from Changchun New Industries Co., Ltd., China). Fourier transform infrared (FTIR) spectra were confirmed by Nicolet iS10 FT-IR spectrometer (Thermo scientific, America) in the wavenumber range of 4,000–400 cm^{-1} with the ATR plugin.

2.3 Synthesis of core UCNPs ($LiErF_4$ and $LiErF_4$: 0.5% Tm^{3+} core nanoparticles)

The UCNPs were synthesized by referring to the methods in the previous literature with some modifications [38]. $ErCl_3·6H_2O$ (1 mmol, 381.71 mg) was placed in a 50 mL three-necked round-bottom flask, then 6 mL OA and 14 mL ODE were added to the three-necked flask and stirred continuously at room temperature. N_2 was flowed for 30 min to remove the air from the reaction system. The solution in the three-neck flask was heated to 160 °C and stirred continuously for 30 min. The reaction solution cooled down to 50 °C naturally at room temperature. A solution of 10 mL methanol containing NH_4F (4 mmol, 148.00 mg) and LiOH (2.5 mmol, 59.88 mg) was added and then heated to 70 °C for 30 min until the methanol in the solution was completely removed. Under the protection of N_2, the solution was heated to 300 °C and maintained for 90 min with stirring. Finally, the core UCNPs were precipitated by acetone and anhydrous ethanol and then dispersed in 8 mL cyclohexane for use. Note that the whole experimental process needs to be carried out under the protection of N_2 atmosphere and continuous stirring. The synthesis of $LiErF_4$: 0.5% Tm^{3+} was similar to that of $LiErF_4$, as long as $ErCl_3·6H_2O$ (1 mmol, 381.71 mg) was replaced by $ErCl_3·6H_2O$ (0.995 mmol, 379.80 mg) and $TmCl_3·6H_2O$ (0.005 mmol, 1.92 mg).

2.4 Synthesis of core–shell UCNPs ($LiErF_4$@$LiYF_4$ and $LiErF_4$: 0.5% Tm^{3+}@$LiYF_4$ core–shell nanoparticles)

The synthetic procedure for the $LiErF_4$@$LiYF_4$ and $LiErF_4$: 0.5% Tm^{3+}@$LiYF_4$ core–shell UCNPs was similar to that of the core with slight differences and is simply described as follows: Briefly, $YCl_3·6H_2O$ (0.75 mmol, 227.52 mg) was added to a mixture of 6 mL OA and 14 mL ODE and stirred continuously at room temperature under N_2 for 30 min. The solution was heated to 160 °C and maintained for 30 min and then cooled down to 30 °C under N_2, a solution of 5 mL methanol containing NH_4F (3 mmol, 111.00 mg) and LiOH (1.875 mmol, 44.90 mg) was added dropwise and after that the solution was heated up to 70 °C for 30 min, after the evaporation of methanol, 4 mL cyclohexane dispersed with the core UCNPs ($LiErF_4$ or $LiErF_4$: 0.5% Tm^{3+}) was added and then heated to 90 °C for 30 min to remove the cyclohexane. Finally, the mixture was quickly heated up to 300 °C and reacted for 60 min, the core–shell UCNPs ($LiErF_4$@$LiYF_4$ or $LiErF_4$: 0.5% Tm^{3+}@$LiYF_4$) were obtained. The UCNPs were washed with acetone and ethanol and dispersed in 4 mL cyclohexane for use. Note that the whole experimental process needs to be carried out under the protection of N_2 atmosphere and continuous stirring.

2.5 Synthesis of BF_4^--modified $LiErF_4$: 0.5% Tm^{3+}@$LiYF_4$ core–shell nanoparticles

The core–shell UCNPs prepared above have oleate ligands on the surface, the UCNPs are hydrophobic and cannot be dispersed in water. Therefore, through ligand exchange, the surface of UCNPs was modified by $NOBF_4$ and the BF_4^- replaced oleate to coordinate on the surface of UCNPs.

Ligand exchange of $LiErF_4$: 0.5% Tm^{3+}@$LiYF_4$ was mainly based on the previous literature with some modifications [39].

$NOBF_4$ (0.4 mmol, 46.72 mg) was added to 10 mL anhydrous DMF for ultrasonic dispersion, and then the core–shell UCNPs ($LiErF_4$: 0.5% Tm^{3+}@$LiYF_4$) dispersed in cyclohexane were added to the above mixture for ultrasound for 15 min, then centrifuged at 12,000 rpm for 20 min. After centrifugation to remove the supernatant, the precipitated UCNPs were re-dispersed in hydrophilic media (DMF, DMSO or acetonitrile).

2.6 Water detection in organic solvents

The anhydrous organic solvents such as DMF (DMSO or acetonitrile), deionized water, and DMF (DMSO or acetonitrile) solution containing BF_4^--modified UCNPs ($LiErF_4$: 0.5% Tm^{3+}@$LiYF_4$) after ligand exchange were mixed into 1 mL detection solution in different proportions (Tables S1 and S2 in the Electronic Supplementary Material (ESM)). The upconversion luminescence spectrum from 400 to 700 nm under 808 nm excitation of the detection solution was obtained by fluorescence spectrometer, and the power of the excitation luminescence is the same.

3 Results and discussion

3.1 Synthesis of core ($LiErF_4$) and core–shell ($LiErF_4$@$LiYF_4$) nanoparticles

We first prepared the $LiErF_4$ core nanoparticles, followed by coating with an inert shell of $LiYF_4$. Powder X-ray diffraction pattern confirms a pure tetragonal phase of the as-prepared core ($LiErF_4$) and core–shell ($LiErF_4$@$LiYF_4$) nanoparticles (JCPDS. No. 51-1618) (Fig. 1(a)). A representative TEM image shows high mono-dispersity and tetragonal bipyramidal morphology of the obtained particles (Figs. 1(b) and 1(c)). The $LiErF_4$ core and $LiErF_4$@$LiYF_4$ core–shell nanoparticles are confirmed as (17.2 ± 0.6) nm × (12.6 ± 0.7) nm (long length × short diagonal length) and (27.2 ± 0.7) nm × (17.3 ± 0.9) nm, respectively. The high-resolution TEM images of both core and core–shell nanoparticles demonstrate the lattice fringe of (101) planes with *d*-spacing of 0.47 nm, which is in accordance with that of tetragonal-phased $LiErF_4$ counterpart.

The comparisons of upconversion (UC) emission between Er^{3+} singly doped bare core ($LiYF_4$: *x*% Er^{3+}, *x*: 2–100) and core-inert shell ($LiYF_4$: *x*% Er^{3+}@$LiYF_4$, *x*: 2–100) nanoparticles have been conducted (Fig. S1 in the ESM). In the bare core structure, with increasing of the doping concentration of Er^{3+} ions, the UC emission dramatically decreased and the $LiErF_4$ bare core exhibited no emission at all. Because in $LiErF_4$ bare core system, the very short distance between the activator Er^{3+} ions leads to rapid energy migration and cross relaxation (CR) process, which further induces the serious energy dissipation from the activators Er^{3+} ions to the surface quenching sites of the bare core nanoparticles (concentration quenching effect). However, after the $LiYF_4$ shell coating, the red UC emission gradually enhanced with the increase of the doping concentration and the optimal concentration could be promoted to 100%, which overcame the concentration quenching and the UC emission can be achieved in this $LiErF_4$@$LiYF_4$ core–shell

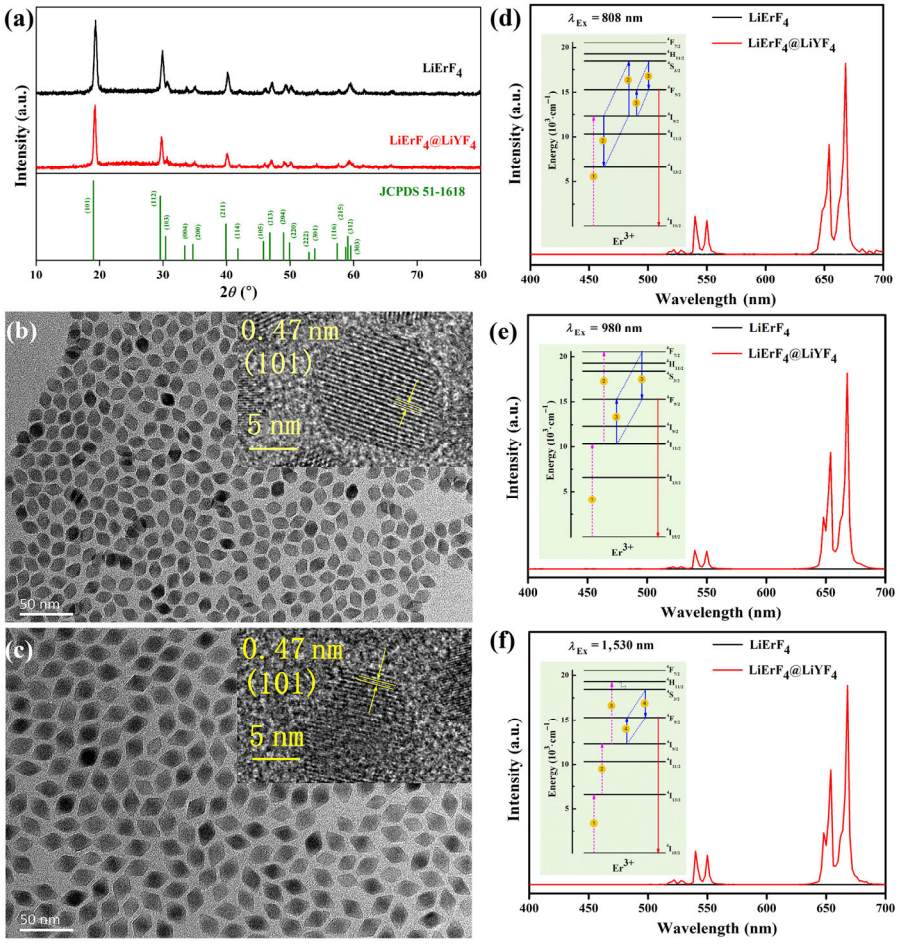

Figure 1 (a) XRD patterns of $LiYF_4$ based UCNPs. The low-resolution TEM and high-resolution TEM (inset) images of (b) $LiErF_4$ bare core and (c) $LiErF_4$@$LiYF_4$ core–shell nanoparticles in cyclohexane. Upconversion emission spectra of $LiErF_4$ and $LiErF_4$@$LiYF_4$ in cyclohexane under (d) 808 nm excitation (0.56 W), (e) 980 nm excitation (3.86W), and (f) 1,530 nm excitation (0.73W), respectively. The energy level diagrams of Er^{3+} ions as well as the proposed CR mechanisms in nanostructures were also inserted.

structure, as indicated in Figs. 1(d)–1(f). Unlike the traditional sensitizer and activator co-doping systems, which usually only work effectively on one specific excitation wavelength, in $LiErF_4$@$LiYF_4$ core–shell nanostructures, Er^{3+} ions act as both sensitizers and activators. They exhibit UC emission under multi-band NIR wavelength (e.g., ~ 808, ~ 980, and ~ 1,530 nm) excitation due to the unique ladder-like energy levels of Er^{3+} ions.

The green (520–575 nm) and red (640–675 nm) emissions are assigned to $(^2H_{11/2}, {}^4S_{3/2}) \rightarrow {}^4I_{15/2}$ and $^4F_{9/2} \rightarrow {}^4I_{15/2}$ transitions of Er^{3+} in $LiErF_4$@$LiYF_4$ nanoparticles. It is worth noting that the UC emission of $LiErF_4$@$LiYF_4$ nanostructure always has a relatively high red/green (R/G) ratio (over 10.7 under 980 nm excitation) within the visible spectrum. This characteristic can be attributed to the efficient interactions between Er^{3+} ions [40–42], i.e., CR_{808ex}: $2\ {}^4I_{9/2} \rightarrow {}^4S_{3/2} + {}^4I_{13/2}$ and $^4S_{3/2} + {}^4I_{9/2} \rightarrow 2\ {}^4F_{9/2}$, CR_{980ex}: $^4F_{7/2} + {}^4I_{11/2} \rightarrow 2\ {}^4F_{9/2}$ and CR_{1530ex}: $^4S_{3/2} + {}^4I_{9/2} \rightarrow 2\ {}^4F_{9/2}$ (inset in Figs. (d)–1(f)).

3.2 Synthesis of core ($LiErF_4$: 0.5% Tm^{3+}) and core–shell ($LiErF_4$: 0.5% Tm^{3+}@$LiYF_4$) nanoparticles

Although in $LiErF_4$@$LiYF_4$ system, the design of the inert shell coating can significantly suppress the concentration quenching dominated by energy migration to surface defects, the luminescence quenching caused by the rapid energy migration among Er^{3+} ions to internal lattice defects cannot be restrained simply by this surface coating method. We further introduced 0.5% Tm^{3+} as a transient energy trapping center into the $LiErF_4$ core to confine the excitation energy and minimize the migration-mediated energy loss in the lattice [27, 43].

As shown in Figs. 2(a)–2(c), tetragonal phase core and core–shell nanoparticles ($LiErF_4$: 0.5% Tm^{3+} and $LiErF_4$: 0.5% Tm^{3+}@$LiYF_4$) exhibit a mean size of (17.4 ± 0.5) × (13.2 ± 0.8) nm and (27.2 ± 0.9) × (17.4 ± 0.8) nm, respectively, similar with the size of those nanocrystals without 0.5% Tm^{3+} dopants. The luminescence spectra of $LiErF_4$: 0.5% Tm^{3+} core and $LiErF_4$: 0.5% Tm^{3+}@$LiYF_4$ core–shell nanoparticles dispersed in cyclohexane were given in Figs. 2(d)–2(f). It can be seen that the UC emission of the $LiErF_4$: 0.5% Tm^{3+} core nanocrystals shows a severe quenching phenomenon, which indicates a high level of energy migration to surface defects. Compared with $LiErF_4$@$LiYF_4$, the green UC emission intensities of $LiErF_4$: 0.5% Tm^{3+}@$LiYF_4$ were decreased, while the red UC emission intensities increased significantly under different excitations. The R/G ratios were enhanced by a factor of 12 times for 808 nm excitation, 20 times for 980 nm excitation, and 11 times for 1,530 nm excitation, respectively, thus achieving strong monochromic red emission (Fig. 3(a)). These results demonstrated that the Tm^{3+} doping results in the re-populating of the red emitting level of Er^{3+} ($^4F_{9/2}$). In $LiErF_4$@$LiYF_4$ system, the $^4F_{9/2}$ energy level is mainly populated by the cross-relaxation progress between Er^{3+} ions (CR_{808ex}: $2\ {}^4I_{9/2} \rightarrow {}^4S_{3/2} + {}^4I_{13/2}$ and $^4S_{3/2} + {}^4I_{9/2} \rightarrow 2\ {}^4F_{9/2}$) as shown in Fig. 1(d). However, in the case of $LiErF_4$: 0.5% Tm^{3+}@$LiYF_4$ system, as indicated in Fig. 3(b), the population of one 808 nm photon at the $^4I_{9/2}$ energy level of Er^{3+} ions can be realized by direct excitation (Step 1) or through energy transfer from an adjacent Er^{3+} ion. Subsequently, the energy distribution of $^4I_{11/2}$ energy level of Er^{3+} ions mainly comes from the multi-phonon non-radiative relaxation (MPR) of $^4I_{9/2}$ energy level and the energy transfer process from the $^4I_{11/2}$ energy level of the adjacent Er^{3+} ions. The electronic structure of Tm^{3+} facilitates downhill energy transfer from the $^4I_{11/2}$ and $^4I_{13/2}$ energy levels of Er^{3+} ions to the $^3H_5$ and $^3F_4$ energy levels of Tm^{3+} ions, respectively (Step 2). Hence, a large amount of the energy in the $^4I_{11/2}$ and $^4I_{13/2}$ level of Er^{3+} ions is transferred to the $^3H_5$ and $^3F_4$ energy levels of Tm^{3+} ions. Notably, the optimal 0.5% Tm^{3+} doping enables a relatively small reduction in energy interval and allows the excited electrons to be accumulated in favor of excited-state population, which minimizes energy migration to particle surface and promotes trapping of the excitation energy [27]. Thus, the transferred energy is effectively stored in these Tm^{3+} energy levels and eventually promotes the population of the red-emitting $^4F_{9/2}$ energy level of Er^{3+} ions via energy transfer upconversion (Step 3), achieving strong and monochromic red UC emission (Step 4).

Coating inert $LiYF_4$ shell to the nonluminous $LiErF_4$ core can not only effectively suppress the surface-related quenching, but also eliminate the concentration quenching. Through the

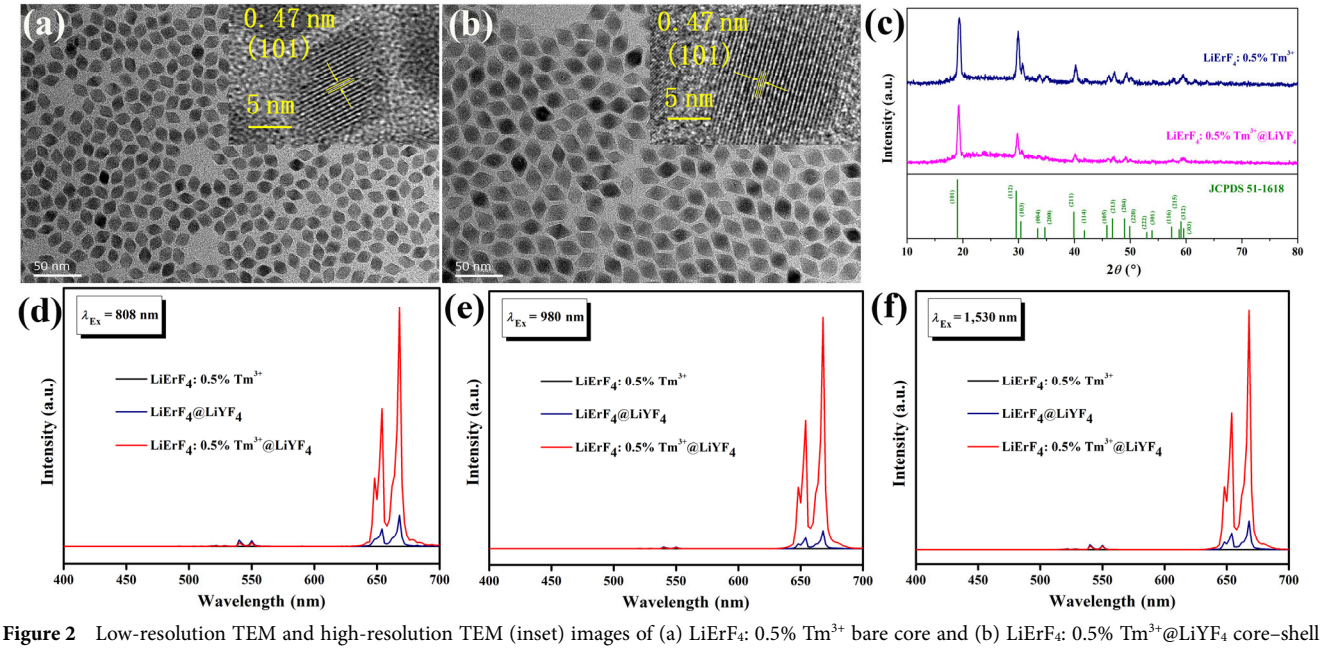

Figure 2 Low-resolution TEM and high-resolution TEM (inset) images of (a) $LiErF_4$: 0.5% Tm^{3+} bare core and (b) $LiErF_4$: 0.5% Tm^{3+}@$LiYF_4$ core–shell nanoparticles in cyclohexane. (c) XRD patterns of $LiErF_4$: 0.5% Tm^{3+} based UCNPs. Upconversion emission spectra of $LiErF_4$: 0.5% Tm^{3+}, $LiErF_4$@$LiYF_4$, and $LiErF_4$: 0.5% Tm^{3+}@$LiYF_4$ in cyclohexane under different excitations: (d) 808 nm excitation (0.56W), (e) 980 nm excitation (3.86W), and (f) 1,530 nm excitation (0.73W).

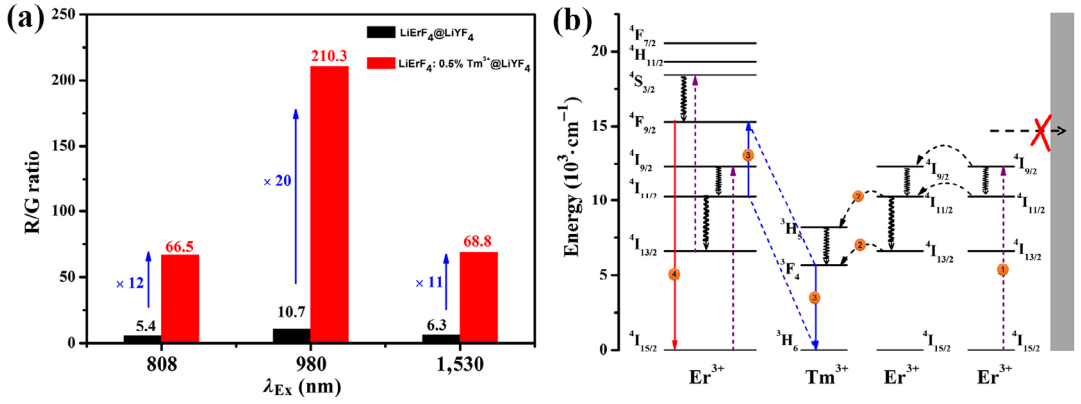

Figure 3 (a) R/G ratios of $LiErF_4$@$LiYF_4$ and $LiErF_4$: 0.5% Tm^{3+}@$LiYF_4$ under 808, 980, and 1,530 nm excitation, respectively. (b) Schematic diagram of the energy transfer process between Er^{3+} and Tm^{3+}. The dashed purple, solid red, dashed black, solid blue, and wavy black arrows represent photon excitation, emission, energy transfer, cross relaxation, and non-radiative relaxation, respectively.

use of 0.5% Tm^{3+} dopants into the core, the luminescence quenching effect, dominated by the fast energy migration among Er^{3+} ions, could also be maximally minimized. With all these efforts, we set up a $LiErF_4$: 0.5% Tm^{3+}@$LiYF_4$ upconverison nano-system with enriched Er^{3+} ions and bright monochromic red UC emission under multi-band NIR excitation (e.g., ~ 808, ~ 980, and ~ 1,530 nm). As a proof of concept, we further demonstrated the as-designed $LiErF_4$: 0.5% Tm^{3+}@$LiYF_4$ nanoparticle as a very sensitive probe for trace water sensing.

3.3 Characterization of BF_4^--modified $LiErF_4$: 0.5% Tm^{3+}@$LiYF_4$ nanoparticles

The surface ligands of $LiErF_4$: 0.5% Tm^{3+}@$LiYF_4$ nanoparticles and oleic acids, were removed by $NOBF_4$ treatment and converted into hydrophilicity. Then the BF_4^--modified nanoparticles could be dissolved in various organic solvents, so that they can absorb water molecules for water detection. Compared with the FTIR spectrum of the untreated UCNPs, the C–H stretching vibrations at 2,800–3,000 cm^{-1} and stretching vibrations of the carboxylic group at 1,577 and 1,452 cm^{-1} disappeared in the FTIR spectrum of the BF_4^--modified nanoparticles (Fig. 4(a)), confirming the removal of surface ligand OA. A new peak at ~ 1,084 cm^{-1} appears after ligand exchange, which is ascribe to BF_4^- anions. And another new peak at ~ 1,650 cm^{-1} belongs to the C=O stretching vibrations of the solvent DMF molecules. Besides, the size and crystal phase of the particles did not change after ligand exchange (Fig. 4(b) and Fig. S2 in the ESM). These results show that BF_4^--modified UCNPs were modified successfully into hydrophilicity by $NOBF_4$ treatment and can be further used for water detection.

3.4 Detection of water in organic solvents

We demonstrate the water sensing in DMF, DMSO, and acetonitrile organic solvents, respectively. A series of testing solutions containing BF_4^--modified $LiErF_4$: 0.5% Tm^{3+}@$LiYF_4$ nanoparticles and different amounts of water were prepared (see details in Tables S1 and S2 in the ESM). Upon exciting these organic solutions by 808 nm laser, which can reduce the thermal effect and improve the accuracy and sensitivity of the detection, we found that the red emission of all samples were gradually quenched with the increase of water contents in test solutions (Figs. 5(a)–5(c)). The relationships between the integrated red emission (640–675 nm) intensities and water contents are depicted in Figs. 5(d)–5(f). In fact, the luminescence quenching data for a certain water content can be linearly fitted according to the following equation:

$$F/F_0 = K \log [H_2O\ (vol.\%)] + B \quad (1)$$

where K represents the slope of the fitted curve. The physical meaning of K is the sensitivity of $LiErF_4$: 0.5% Tm^{3+}@$LiYF_4$ upconversion nanoprobes to water molecules in organic solvents. The larger the absolute value of K ($|K|$) is, the easier the red UC emission of the nanoprobes be quenched by water, and the more sensitive the nanoprobes response to water molecules. [H_2O (vol.%)] is the volume fraction of H_2O in organic solvents, B is a constant, and F_0 and F are the integrated red emission (640–675 nm) intensities in the absence and presence of H_2O, respectively. The relative intensity of UC emission (F/F_0) was indeed linearly dependent on the water content but exhibited two-separated linearity with logarithm of water concentration (vol.%) at the low water content and high water content intervals, respectively, as indicated in Figs. 5(d)–5(f), which indicated a nonlinear quenching effect.

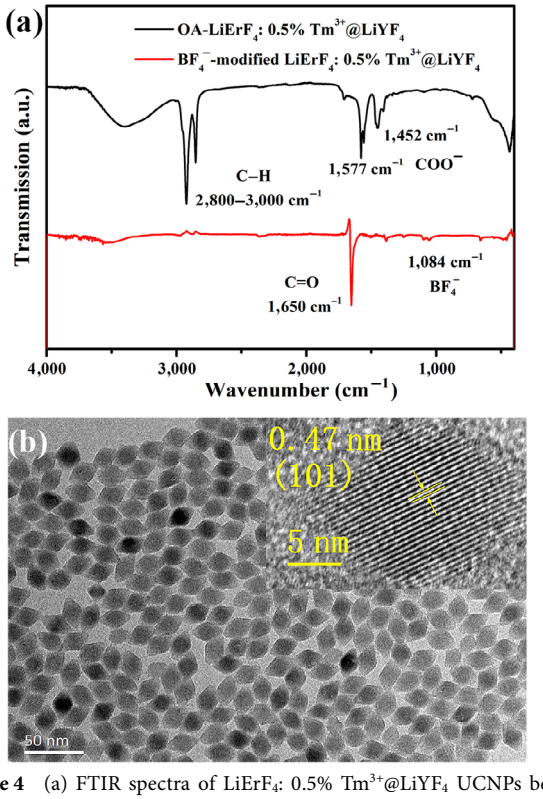

Figure 4 (a) FTIR spectra of $LiErF_4$: 0.5% Tm^{3+}@$LiYF_4$ UCNPs before and after ligand exchange. (b) Resolution TEM and high-resolution TEM (inset) images of the BF_4^--modified $LiErF_4$: 0.5% Tm^{3+}@$LiYF_4$ core–shell UCNPs dispersed in DMF.

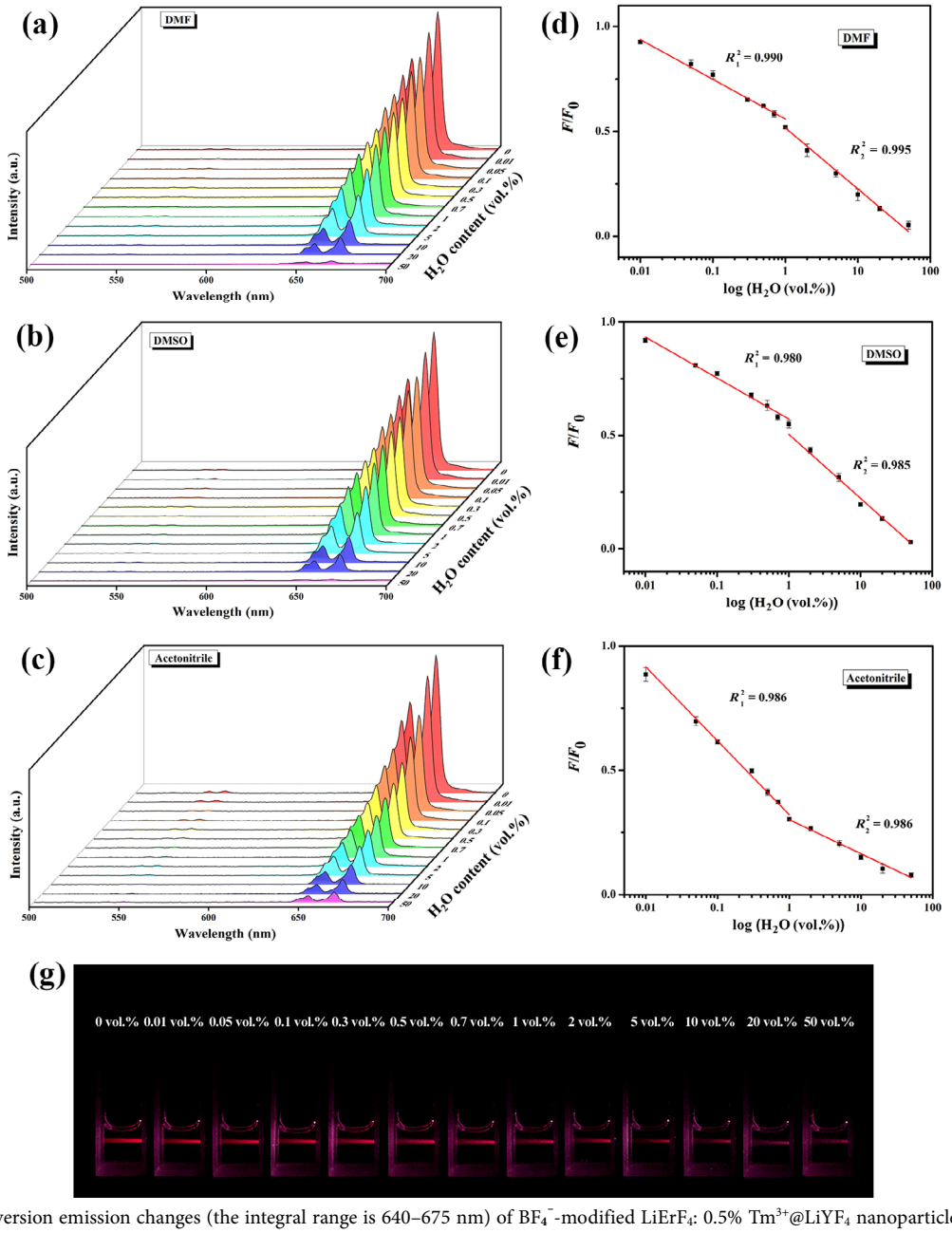

Figure 5 Upconversion emission changes (the integral range is 640–675 nm) of BF_4^--modified $LiErF_4$: 0.5% Tm^{3+}@$LiYF_4$ nanoparticles dispersed in (a) DMF, (b) DMSO, and (c) acetonitrile with different water contents (0 vol.%–50 vol.%) under 808 nm excitation (1.42 W). Corresponding F/F_0 dependence on H_2O concentration of $LiErF_4$: 0.5% Tm^{3+}@$LiYF_4$ nanoparticles dispersed in (d) DMF, (e) DMSO, and (f) acetonitrile. (g) Corresponding luminescent photographs of the probes in acetonitrile containing water with different contents.

It is worth noting that in the solution of DMF and DMSO, the $|K|$ in high water content is larger than that in low water content, while that of acetonitrile solution is opposite. The proposed mechanism is illustrated in Scheme 1. After surface modification, the BF_4^--modified $LiErF_4$: 0.5% Tm^{3+}@$LiYF_4$ nanoparticles exhibit positive charge, which attributed to the uncoordinated rare earth metal Er^{3+} cations arising from the removal of organic ligands [39]. The electron cloud density of oxygen atom (O) in DMF or DMSO molecules is higher than that of nitrogen atom (N) in acetonitrile, so the interaction between the DMF or DMSO molecules and the BF_4^--modified nanoparticles is stronger than that in acetonitrile molecules. When the water content is low, due to the shielding effect of the inner DMF or DMSO molecules, the water molecules are far away from the Er^{3+} emission centers, so it is not easy to quench the luminescence, leading to the relatively small $|K|$. With the increase of water contents, more and more water molecules accumulate around the probe nanoparticles, thus the quenching effect is enhanced, and the $|K|$ becomes bigger. While in acetonitrile solutions, owing to the weak interaction between acetonitrile molecules and BF_4^--modified $LiErF_4$: 0.5% Tm^{3+}@$LiYF_4$ nanoparticles, water molecules are more easily diffused and adsorbed on the surface of probe nanoparticles, resulting in the significantly quenching of the luminescence at very low water content. With the increase of water content, the water molecules on the surface of nanoparticles reach saturation, the quenching effect becomes weak, resulting in a relatively small $|K|$. The limits of detection (LOD) in DMF, DMSO, and acetonitrile were calculated to be as low as 58, 50, and 30 ppm, respectively, based on the formula $3\sigma/|K|$, where σ is the standard deviation of the response using the UCNPs solution containing 0.01 vol.% water as the reference.

Next, we studied the photostability of BF_4^--modified $LiErF_4$: 0.5% Tm^{3+}@$LiYF_4$ nanoprobes and the stability of luminescent

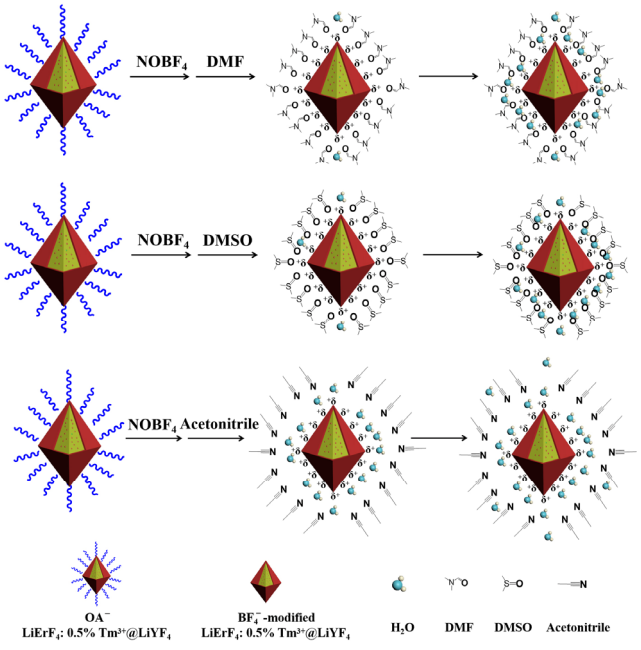

Scheme 1 Proposed water sensing mechanism of BF_4^--modified $LiErF_4$: 0.5% Tm^{3+}@$LiYF_4$ nanoparticles in DMF, DMSO, and acetonitrile, respectively with different solvents.

signals response to the addition of water. As can be seen in Fig. S3 in the ESM, in a testing solution (H_2O/DMF, 5 vol.%/95 vol.%), the red UC emission quickly became stable and stayed almost the same after 60 min of 808 nm laser excitation. We further continuously recorded the red UC emission upon different contents of water addition. A steady response was obtained within 1 min as indicated by the stable step curve in Fig. 6, demonstrating the possibility for *in situ* water monitoring. In the following experiment, we introduced various organic dyes as disruptors to check the antijamming capability of these nanoprobes. Benefiting from the near-infrared excitation, no obvious interference was observed when the testing solution contained impurities, such as 9-(diethylamino)-5H-benzo [a] phenoxazin-5-one (Nile Red), 4, 4-difluoro-1, 3, 5, 7, 8-pentamethyl-4-bora-3a, 4a-diaza-s-indacene (BODIPY), dimethyl 2, 5-bis(methylamino)terephthalate (Ph-C_1), and 5,12-dibutyl-5,12-dihydroquinolino[2, 3-b]acridine-7, 14-dione (C_4-QA) (Fig. S4 in the ESM). However, the presence of organic dyes could largely affect the performance of typical organic luminescent molecules based optical water sensors which are mainly excited by ultraviolet light owing to the intrinsic fluorescence nature. In addition, we have studied the selectivity as can be seen in Fig. S5 in the ESM. The red UC emission intensity of $LiErF_4$: Tm^{3+}@$LiYF_4$ nanoprobe remains almost the same when DMF (blank), acetone, DMSO, and acetonitrile were added. While the intensity decreased slightly in ethanol, and significantly in water. Both water and ethanol caused varying degrees of reduction in UC emission because of the high energy (ca. 3,500 cm^{-1}) of O–H stretching vibration which could quench the luminescence of Er^{3+} ions [22, 23]. However, ethanol molecule has one OH-group, and the water molecule has two. When the concentration of water and ethanol in organic solvent is the same, the number of OH-groups in water is more than that in ethanol. Therefore, the nanoprobe is much more sensitive to water molecules. Moreover, in a testing solution (H_2O/DMF, 5 vol.%/95 vol.%), after 4 reaction cycles (Fig. S6 in the ESM), the change of F/F_0 still maintained a relatively stable value. These results reveal that the BF_4^--modified $LiErF_4$: 0.5% Tm^{3+}@$LiYF_4$ nanoprobes are suitable for long-term, real-time, and *in situ* monitoring of water content, even in complex samples.

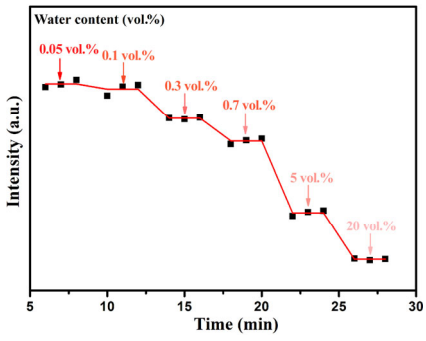

Figure 6 Upconversion emission response to the different water contents in DMF testing solution within 30 min, under continuous 808 nm laser excitation (1.42 W). The solid red arrows indicate the addition of water.

3.5 Proposed energy transfer quenching mechanisms for water detection

In order to clarify the quenching effect of water molecules on the UC emission of BF_4^--modified $LiErF_4$: 0.5% Tm^{3+}@$LiYF_4$ nanoparticles, the decay curves of excited states ($^4F_{9/2} \rightarrow {}^4I_{15/2}$, $^4I_{11/2} \rightarrow {}^4I_{15/2}$, and $^4I_{13/2} \rightarrow {}^4I_{15/2}$ transition) dispersed in DMF solutions with different water contents were measured (Fig. 7 and Figs. S7 and S8 in the ESM). The life time of each emitting state calculated by fitting is also listed in Table 1. The results show that with the increase of water content in the DMF solution, the lifetime of each excited state becomes shorter, indicating an increased non-radiative relaxation of the excited states ascribed to high energy vibrational modes of OH-groups, as illustrated in Scheme 2. We found that the O–H stretching vibration mode in water molecule is ca. 3,500 cm^{-1}. The energy band gap of $^4F_{9/2} \rightarrow {}^4I_{9/2}$ energy levels and the gap of $^4I_{11/2} \rightarrow {}^4I_{13/2}$ energy levels in Er^{3+} ions are ca. 3,000 and 3,700 cm^{-1},

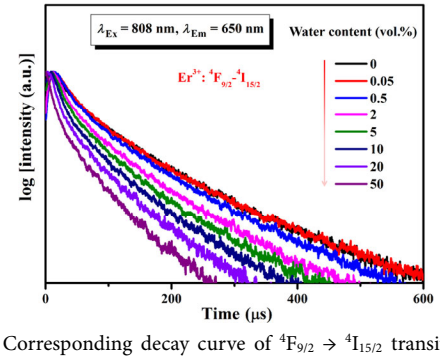

Figure 7 Corresponding decay curve of $^4F_{9/2} \rightarrow {}^4I_{15/2}$ transition of Er^{3+} under 808 nm excitation (1.42 W).

Table 1 Lifetime of $^4F_{9/2}$, $^4I_{11/2}$, and $^4I_{13/2}$ levels in DMF solution with different water contents under 808 nm excitation

Water content (vol.%)	Lifetime (μs)		
	$^4F_{9/2}$	$^4I_{11/2}$	$^4I_{13/2}$
0	119	317	1,074
0.05	115	307	1,052
0.5	105	289	1,048
2	85	259	949
5	76	241	923
10	65	222	864
20	53	206	828
50	44	201	636

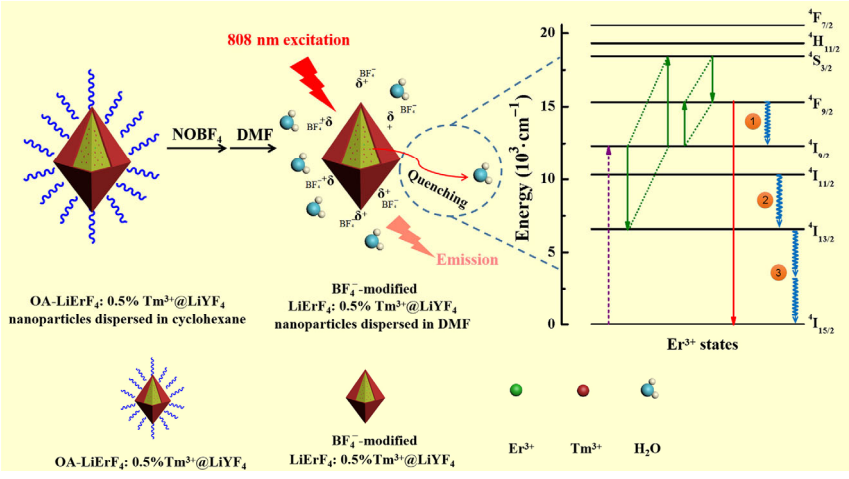

Scheme 2 Proposed energy transfer quenching mechanism in $LiErF_4$: 0.5% Tm^{3+}@$LiYF_4$ core–shell UCNPs for water detection.

respectively [44], which are close to one O–H stretching mode. As a result, the energy distributed at $^4F_{9/2}$ and $^4I_{11/2}$ energy level could directly be quenched through facilitating multi-phonon relaxation by water molecules under 808 nm excitation, leading to the decrease of the lifetime of 650 and 980 nm, as demonstrated in Steps 1 and 2 in Scheme 2. Moreover, the energy interval between $^4I_{13/2}$ and $^4I_{15/2}$ is about 6,600 cm^{-1} [44], which is close to a couple of O–H stretching modes. Therefore, two OH-groups can make Er^{3+} ion relax from $^4I_{13/2}$ level to $^4I_{15/2}$ ground state without radiation, as indicated in Step 3, and the luminescence lifetime of $^4I_{13/2}$ excited state decreased. This effect of the OH-vibrations was also confirmed by the measurement of luminescence spectra of $^4I_{11/2}$ and $^4I_{13/2}$ level under 808 nm excitation, as shown in Figs. S9 and S10 in the ESM. Due to the non-radiation transition of $^4I_{11/2} \rightarrow {}^4I_{13/2}$ and $^4I_{13/2} \rightarrow {}^4I_{15/2}$, the population of $^4I_{11/2}$ and $^4I_{13/2}$ level decreased and the intensity of emission decreased gradually. Therefore, the sensitive response of water can be achieved through testing the change of the monochromatic red emission in Er^{3+} ions enriched $LiErF_4$: 0.5% Tm^{3+}@$LiYF_4$ core–shell nanoparticles.

4 Conclusions

In conclusion, we have established a red upconversion emission system based on $LiErF_4$, i.e., $LiErF_4$@$LiYF_4$ and its relevant derivative $LiErF_4$: 0.5% Tm^{3+}@$LiYF_4$. Simply coating inert $LiYF_4$ shell to the nonluminous $LiErF_4$ core can not only effectively suppress the surface-related quenching, but also eliminate the concentration quenching, making $LiErF_4$ glow. Through the use of 0.5% Tm^{3+} dopants into $LiErF_4$ core, the luminescence quenching effect, dominated by the fast energy migration in the $LiErF_4$ host lattice, could also be maximally minimized. With all these efforts, a strong and monochromic red emission under multi-band NIR excitation (e.g., ~ 808, ~ 980, and ~ 1,530 nm) could be achieved by this simple core–shell nanostructure. The Er^{3+} ions enriched nature makes $LiErF_4$: 0.5% Tm^{3+}@$LiYF_4$ nanoparticles very sensitive for trace water sensing in organic solvent with detection limit of 30 ppm in acetonitrile, 50 ppm in DMSO, and 58 ppm in DMF under safe excitation of 808 nm. Benefiting from their superior chemical and physical stability, the designed $LiErF_4$: 0.5% Tm^{3+}@$LiYF_4$ nanoprobes could be used for real-time and long-term water monitoring in challenging conditions. In addition, water probing was created as a proof of concept and did not cover all usage scenarios. We believe that the unique property of monochromic red emission under multi-band NIR excitations could also endow these $LiErF_4$ based materials potential for solar cells and anti-counterfeiting application, etc.

Acknowledgements

This work was financially supported by the Science and Technology Development Program of Jilin Province (No. 20170520162JH), the National Key Research and Development Program of China (No. 016YFC0207300), the National Natural Science Foundation of China (Nos. 61875191, 11874354, 61722305, and 61833006), the Program for Jilin University Science and Technology Innovative Research Team (No. JLUSTIRT 2017TD-07), Jilin Development and Reform Commission (No. 2018C052-10), and the Open Project of State Key Laboratory of Supramolecular Structure and Materials (No. sklssm202023).

Electronic Supplementary Material: Supplementary material (preparation of detection solutions with different water contents (Tables S1 and S2), UC emission spectra of $LiYF_4$: *x*% Er (*x*: 2–100) bare core and $LiYF_4$: *x*% Er (*x*: 2–100)@$LiYF_4$ core–shell nanoparticles (Fig. S1), XRD pattern (Fig. S2), photostability of BF_4^--modified nanocrystals (Fig. S3), antijamming performance (Fig. S4), the selectivity test (Fig. S5), circulation utilization rate test (Fig. S6), and lifetime and emission measurement of $^4I_{11/2} \rightarrow {}^4I_{15/2}$ and $^4I_{13/2} \rightarrow {}^4I_{15/2}$ transition of Er^{3+} under 808 nm excitation (Figs. S7–S10)) is available in the online version of this article at https://doi.org/10.1007/s12274-020-2932-4.

References

[1] Wang, L. Y.; Li, Y. D. Luminescent coordination compound nanospheres for water determination. *Small* **2007**, *3*, 1218–1221.

[2] Nussbaum, R.; Lischke, D.; Paxmann, H.; Wolf, B. Quantitative GC determination of water in small samples. *Chromatographia* **2000**, *51*, 119–121.

[3] Lee, W.; Jin, Y. J.; Park, L. S.; Kwak, G. Fluorescent actuator based on microporous conjugated polymer with intramolecular stack structure. *Adv. Mater.* **2012**, *24*, 5604–5609.

[4] Dantan, N.; Frenzel, W.; Kuppers, S. Determination of water traces in various organic solvents using Karl Fischer method under FIA conditions. *Talanta* **2000**, *52*, 101–109.

[5] Men, G. W.; Zhang, G. R.; Liang, C. S.; Liu, H. L.; Yang, B.; Pan, Y. Y.; Wang, Z. Y.; Jiang, S. M. A dual channel optical detector for trace water chemodosimetry and imaging of live cells. *Analyst* **2013**, *138*, 2847–2857.

[6] Yang, X.; Niu, C. G.; Shang, Z. J.; Shen, G. L.; Yu, R. Q. Optical-fiber sensor for determining water content in organic solvents. *Sens. Actuators B Chem.* **2001**, *75*, 43–47.

[7] Citterio, D.; Minamihashi, K.; Kuniyoshi, Y.; Hisamoto, H.; Sasaki, S. I.; Suzuki, K. Optical determination of low-level water concentrations in organic solvents using fluorescent acridinyl dyes and dye-immobilized polymer membranes. *Anal. Chem.* **2001**, *73*, 5339–5345.

[8] Ding, L.; Zhang, Z. Y.; Li, X.; Su, J. H. Highly sensitive determination of low-level water content in organic solvents using novel solvatochromic dyes based on thioxanthone. *Chem. Commun.* **2013**, *49*, 7319–7321.

[9] Jung, H. S.; Verwilst, P.; Kim, W. Y.; Kim, J. S. Fluorescent and colorimetric sensors for the detection of humidity or water content. *Chem. Soc. Rev.* **2016**, *45*, 1242–1256.

[10] Yao, M. Z.; Chen, W. Hypersensitive luminescence of Eu^{3+} in dimethyl sulfoxide as a new probing for water measurement. *Anal. Chem.* **2011**, *83*, 1879–1882.

[11] Deng, Q. L.; Li, Y. L.; Wu, J. H.; Liu, Y.; Fang, G. Z.; Wang, S.; Zhang, Y. K. Highly sensitive fluorescent sensing for water based on poly (*m*-aminobenzoic acid). *Chem. Commun.* **2012**, *48*, 3009–3011.

[12] Guo, S. H.; Xie, X. J.; Huang, L.; Huang, W. Sensitive water probing through nonlinear photon Upconversion of lanthanide-doped nanoparticles. *ACS Appl. Mater. Interfaces* **2016**, *8*, 847–853.

[13] Chen, D. Q.; Xu, M.; Huang, P.; Ma, M. F.; Ding, M. Y.; Lei, L. Water detection through Nd^{3+}-sensitized photon upconversion in core-shell nanoarchitecture. *J. Mater. Chem. C* **2017**, *5*, 5434–5443.

[14] Wang, W.; Zhao, M. Y.; Wang, L; Chen, H. Q. Core-shell upconversion nanoparticles of type $NaGdF_4$: Yb, Er@$NaGdF_4$: Nd, Yb and sensitized with a NIR dye are a viable probe for luminescence determination of the fraction of water in organic solvents. *Microchim. Acta* **2019**, *186*, 630.

[15] Xu, J. T.; Gulzar, A.; Yang, P. P.; Bi, H. T.; Yang, D.; Gai, S. L.; He, F.; Lin, J.; Xing, B. G.; Jin, D. Y. Recent advances in near-infrared emitting lanthanide-doped nanoconstructs: Mechanism, design and application for Bioimaging. *Coord. Chem. Rev.* **2019**, *381*, 104–134.

[16] Wen, S. H.; Zhou, J. J.; Zheng, K. Z.; Bednarkiewicz, A.; Liu, X. G.; Jin, D. Y. Advances in highly doped upconversion nanoparticles. *Nat. Commun.* **2018**, *9*, 2415.

[17] Dong, H.; Du, S. R.; Zheng, X. Y.; Lyu, G. M.; Sun, L. D.; Li, L. D.; Zhang, P. Z.; Zhang, C.; Yan, C. H. Lanthanide nanoparticles: From design toward bioimaging and therapy. *Chem. Rev.* **2015**, *115*, 10725–10815.

[18] Chen, G. Y.; Qiu, H. L.; Prasad, P. N.; Chen, X. Y. Upconversion nanoparticles: Design, nanochemistry, and applications in theranostics. *Chem. Rev.* **2014**, *114*, 5161–5214.

[19] Gai, S.; Li, C.; Yang, P.; Lin, J. Recent progress in rare earth micro/nanocrystals: Soft chemical synthesis, luminescent properties, and biomedical applications. *Chem. Rev.* **2014**, *114*, 2343–2389.

[20] Li, X. M.; Zhang, F.; Zhao, D. Y. Lab on upconversion nanoparticles: Optical properties and applications engineering via designed nanostructure. *Chem. Soc. Rev.* **2015**, *44*, 1346–1378.

[21] Tu, L. P.; Liu, X. M.; Wu, F.; Zhang, H. Excitation energy migration dynamics in upconversion nanomaterials. *Chem. Soc. Rev.* **2015**, *44*, 1331–1345.

[22] Wang, F.; Wang, J.; Liu, X. G. Direct evidence of a surface quenching effect on size-dependent luminescence of upconversion nanoparticles. *Angew. Chem., Int. Ed.* **2010**, *49*, 7456–7460.

[23] Arppe, R.; Hyppänen, I.; Perälä, N.; Peltomaa, R.; Kaiser, M.; Wurth, C.; Christ, S.; Resch-Genger, U.; Schäferling, M.; Soukka, T. Quenching of the upconversion luminescence of $NaYF_4$: Yb^{3+}, Er^{3+} and $NaYF_4$: Yb^{3+}, Tm^{3+} nanophosphors by water: The role of the sensitizer Yb^{3+} in non-radiative relaxation. *Nanoscale* **2015**, *7*, 11746–11757.

[24] Haase, M.; Schäfer, H. Upconverting nanoparticles. *Angew. Chem., Int. Ed.* **2011**, 50, 5808–5829.

[25] Chen, G. Y.; Yang, C. H.; Prasad, P. N. Nanophotonics and nanochemistry: Controlling the excitation dynamics for frequency up- and down-conversion in lanthanide-doped nanoparticles. *Acc. Chem. Res.* **2013**, *46*, 1474–1486.

[26] Zuo, J.; Li, Q. Q.; Xue, B.; Li, C. X.; Chang, Y. L.; Zhang, Y. L.; Liu, X. M.; Tu, L. P.; Zhang, H.; Kong, X. G. Employing shells to eliminate concentration quenching in photonic upconversion nanostructure. *Nanoscale* **2017**, *9*, 7941–7946.

[27] Chen, Q. S.; Xie, X. J.; Huang, B. L.; Liang, L. L.; Han, S. Y.; Yi, Z. G.; Wang, Y.; Li, Y.; Fan, D. Y.; Huang, L. et al. Confining excitation energy in Er^{3+}-sensitized upconversion nanocrystals through Tm^{3+}-mediated transient energy trapping. *Angew. Chem., Int. Ed.* **2017**, *56*, 7605–7609.

[28] Zuo, J.; Tu, L. P.; Li, Q. Q.; Feng, Y. S.; Que, I.; Zhang, Y. L.; Liu, X. M.; Xue, B.; Cruz, L. J.; Chang, Y. L. et al. Near infrared light sensitive ultraviolet-blue Nanophotoswitch for imaging-guided "Off-On" therapy. *ACS Nano* **2018**, *12*, 3217–3225.

[29] Na, H. J.; Jeong, J. S.; Chang, H. J.; Kim, H. Y.; Woo, K.; Lim, K.; Mkhoyan, K. A.; Jang, H. S. Facile synthesis of intense green light emitting $LiGdF_4$: Yb, Er-based upconversion bipyramidal nanocrystals and their polymer composites. *Nanoscale* **2014**, *6*, 7461–7468.

[30] Huang, P.; Zheng, W.; Zhou, S. Y.; Tu, D. T.; Chen, Z.; Zhu, H. M.; Li, R. F.; Ma, E.; Huang, M. D.; Chen, X. Y. Lanthanide-doped $LiLuF_4$ Upconversion Nanoprobes for the detection of disease biomarkers. *Angew. Chem., Int. Ed.* **2014**, *53*, 1252–1257.

[31] Mahalingam, V.; Vetrone, F.; Naccache, R.; Speghini, A.; Capobianco, J. A. Colloidal Tm^{3+}/Yb^{3+}-doped $LiYF_4$ nanocrystals: Multiple luminescence spanning the UV to NIR regions via low-energy excitation. *Adv. Mater.* **2009**, *21*, 4025–4028.

[32] Huang, P.; Zheng, W.; Tu, D. T.; Shang, X. Y.; Zhang, M. R.; Li, R. F.; Xu, J.; Liu, Y.; Chen, X. Y. Unraveling the electronic structures of neodymium in $LiLuF_4$ Nanocrystals for ratiometric temperature sensing. *Adv. Sci.* **2019**, *6*, 1802282.

[33] Aebischer, A.; Hostettler, M.; Hauser, J.; Krämer, K.; Weber, T.; Gudel, H. U.; Bürgi, H. B. Structural and spectroscopic characterization of active sites in a family of light-emitting sodium lanthanide tetrafluorides. *Angew. Chem., Int. Ed.* **2006**, *45*, 2802–2806.

[34] Kim, H. J.; Song, J. S.; Kim, S. S. Efficiency enhancement of solar cell by down-conversion effect of Eu^{3+} doped $LiGdF_4$. *J. Korean Phys. Soc.* **2004**, *45*, 609–613.

[35] Wang, F.; Deng, R. R.; Wang, J.; Wang, Q. X.; Han, Y.; Zhu, H. M.; Chen, X. Y.; Liu, X. G. Tuning upconversion through energy migration in core-shell nanoparticles. *Nat. Mater.* **2011**, *10*, 968–973.

[36] Babkevich, P.; Finco, A.; Jeong, M.; Piazza, B. D.; Kovacevic, I.; Klughertz, G.; Krämer, K. W.; Kraemer, C.; Adroja, D. T.; Goremychkin, E. et al. Neutron spectroscopic study of crystal-field excitations and the effect of the crystal field on dipolar magnetism in Li*R*F_4 (*R* = Gd, Ho, Er, Tm, and Yb). *Phys. Rev. B* **2015**, *92*, 144422.

[37] Kraemer, C.; Nikseresht, N.; Piatek, J. O.; Tsyrulin, N.; Dalla Piazza, B.; Kiefer, K.; Klemke, B.; Rosenbaum, T. F.; Aeppli, G.; Gannarelli, C. et al. Dipolar antiferromagnetism and quantum criticality in $LiErF_4$. *Science* **2012**, *336*, 1416–1419.

[38] Johnson, N. J. J.; Korinek, A.; Dong, C. H.; van Veggel, F. C. J. M. Self-focusing by ostwald ripening: A strategy for layer-by-layer epitaxial growth on upconverting nanocrystals. *J. Am. Chem. Soc.* **2012**, *134*, 11068–11071.

[39] Dong, A. G.; Ye, X. C.; Chen, J.; Kang, Y. J.; Gordon, T.; Kikkawa, J. M.; Murray, C. B. A generalized ligand-exchange strategy enabling sequential surface functionalization of colloidal nanocrystals. *J. Am. Chem. Soc.* **2011**, *133*, 998–1006.

[40] Chen, G. Y.; Ohulchanskyy, T. Y.; Kachynski, A.; Ågren, H.; Prasad, P. N. Intense visible and near-infrared upconversion photoluminescence in colloidal $LiYF_4$: Er^{3+} nanocrystals under excitation at 1,490 nm. *ACS Nano* **2011**, *5*, 4981–4986.

[41] Vetrone, F.; Boyer, J. C.; Capobianco, J. A.; Speghini, A.; Bettinelli, M. Concentration-dependent near-infrared to visible upconversion in nanocrystalline and bulk Y_2O_3: Er^{3+}. *Chem. Mater.* **2003**, *15*, 2737–2743.

[42] Shang, X. Y.; Chen, P.; Jia, T. Q.; Feng, D. H.; Zhang, S.; Sun, Z. R.; Qiu, J. R. Upconversion luminescence mechanisms of Er^{3+} ions under excitation of an 800 nm laser. *Phys. Chem. Chem. Phys.* **2015**, *17*, 11481–11489.

[43] Chan, E. M.; Han, G.; Goldberg, J. D.; Gargas, D. J.; Ostrowski, A. D.; Schuck, P. J.; Cohen, B. E.; Milliron, D. J. Combinatorial discovery of lanthanide-doped nanocrystals with spectrally pure upconverted emission. *Nano Lett.* **2012**, *12*, 3839–3845.

[44] Couto dos Santos, M. A.; Antic-Fidancev, E.; Gesland, J. Y.; Krupa, J. C.; Lemaître-Blaise, M.; Porcher, P. Absorption and fluorescence of Er^{3+}-doped $LiYF_4$: Measurements and simulation. *J. Alloys Compd.* **1998**, *275–277*, 435–441.